Nuclear Engineering and Technology 48 (2016) 43–54

Available online at ScienceDirect

Nuclear Engineering and Technology

journal homepage: www.elsevier.com/locate/net

Original Article

Development of Galerkin Finite Element Method Three-dimensional Computational Code for the Multigroup Neutron Diffusion Equation with Unstructured Tetrahedron Elements

*Seyed Abolfazl Hosseini**

Department of Energy Engineering, Sharif University of Technology, Azadi Avenue, Tehran 8639-11365, Iran

ARTICLE INFO

Article history:
Received 28 February 2015
Received in revised form
17 October 2015
Accepted 19 October 2015
Available online 2 December 2015

Keywords:
Finite element method
Forward/adjoint fluxes
Galerkin
Gambit
Power distribution
Unstructured tetrahedron elements

ABSTRACT

In the present paper, development of the three-dimensional (3D) computational code based on Galerkin finite element method (GFEM) for solving the multigroup forward/adjoint diffusion equation in both rectangular and hexagonal geometries is reported. Linear approximation of shape functions in the GFEM with unstructured tetrahedron elements is used in the calculation. Both criticality and fixed source calculations may be performed using the developed GFEM-3D computational code. An acceptable level of accuracy at a low computational cost is the main advantage of applying the unstructured tetrahedron elements. The unstructured tetrahedron elements generated with Gambit software are used in the GFEM-3D computational code through a developed interface. The forward/adjoint multiplication factor, forward/adjoint flux distribution, and power distribution in the reactor core are calculated using the power iteration method. Criticality calculations are benchmarked against the valid solution of the neutron diffusion equation for International Atomic Energy Agency (IAEA)-3D and Water-Water Energetic Reactor (VVER)-1000 reactor cores. In addition, validation of the calculations against the P_1 approximation of the transport theory is investigated in relation to the liquid metal fast breeder reactor benchmark problem. The neutron fixed source calculations are benchmarked through a comparison with the results obtained from similar computational codes. Finally, an analysis of the sensitivity of calculations to the number of elements is performed.

* *Corresponding author.*
E-mail address: sahosseini@sharif.edu.

http://dx.doi.org/10.1016/j.net.2015.10.009
1738-5733/Copyright © 2015, Published by Elsevier Korea LLC on behalf of Korean Nuclear Society.

1. Introduction

Numerical methods have played a vital role in science and engineering in terms of solving and analyzing problems. Solutions to engineering problems can more easily be achieved with the help of computers. The importance of numerical methods in an analysis is due to several factors. First, most natural phenomena can best be described by differential equations with varying boundary conditions the solutions of which cannot be obtained by analytical means, except in very simple cases. Significant improvements have been made in various numerical techniques such that problems can be solved at a low cost and within a short span of time. Due to the absence of automatic computation, progress in the development of numerical methods was quite slow before the 1940s. With the arrival of high-speed computers, engineers and scientists succeeded in exploiting numerical methods. During the mid-1950s, the finite element method grew out of a number of intuitive procedures and associated mathematical techniques. Prior to its conception, the finite difference method held a dominant position in the numerical solution of continuum problems [1,2]. Today, both of these methods are equally important and have their own advantages and disadvantages. However, certain problems are more amenable to the finite element method than to the finite difference method. Other numerical methods, such as nodal [3–5] and finite volume [6,7], may also be used to solve neutron diffusion equations.

The finite element method is a computational technique for obtaining approximate solutions to the partial differential equations that arise in scientific and engineering applications. It is a general technique for constructing approximate solutions to the boundary value problems. The methods involve dividing the domains of a solution into a finite number of elements. Variational schemes employing a weighted residual approach or an extremum principle-based approach are used to construct an approximate solution over the collection of finite elements. Owing to the generality and richness of the ideas underlying the method, it has been used with remarkable success in solving a wide range of problems in virtually all areas of engineering and sciences. In contrast to the older finite difference methods that are usually based on differential formulations, the finite element method is based on integral formulations. In the finite element method, the solution is approximated by local piecewise polynomial trial functions within an element. Expansion coefficients are then determined by applying either weighted residual or variational approaches. Finite elements have been utilized in different ways to solve neutron diffusion equations. In some formulations a weighted residual approach is adopted, while in others variational approaches are considered, with a combination of the applications of the finite elements to one or more of the independent variables. In the weighted residual approach, the integral form of the original integrodifferential equation is considered and expanded in a set of finite element basis functions. The integral form is obtained by multiplying the original equation by an arbitrary weighting function. If the arbitrary weighting functions are the finite element basis functions, then the approach is called the Galerkin technique [8].

The neutron diffusion theory is the most widely used method in the analysis of criticality of nuclear reactors. Consideration of criticality is generally referred to as an eigenvalue problem for the multigroup neutron diffusion equation for which the solution provides the eigenvalue effective multiplication factor, neutron flux distribution, and power profiles in reactor cores. An adequate calculation may be obtained from the solution of a three-dimensional (3D) neutron diffusion equation using the aforementioned numerical methods. The finite element method has always been a fundamental numerical technique in reactor core calculations. It has continuously been improved over decades, starting from primal implementation in neutron diffusion equations up to modern implementations with Raviart–Thomas, hybrid, *h*-adaptivity, and response matrix bases [9–11].

In general, in most applications, the finite element method is preferred to its principal alternative, the finite difference method, due to its flexibility in the treatment of curved or irregular geometries and the high rates of convergence attainable by the use of high-order elements. Several researchers have tried to develop convenient methods for solving 3D multigroup neutron diffusion equations using finite element methods in 3D geometries. For example, Wang and collogues [11] presented 3D *h*-adaptivity for multigroup neutron diffusion equations. The solution of partial differential equations obtained using adaptive mesh refinement gives significantly higher accuracy at a reduced numerical cost. In another paper, Hébert [9] presented how the Raviart–Thomas–Schneider finite element method was implemented for solving the diffusion equation in hexagonal 3D geometry. The Raviart–Thomas–Schneider method was based on a dual variational formulation defined over lozenges with a Piola transformation of the polynomial basis. An efficient Alternating Direction Implicit (ADI) numerical technique was set up to solve the resulting matrix system.

In the present study, the Galerkin finite element method (GFEM) [12], a weighted residual method, is used to solve the multigroup neutron diffusion equation in any arbitrary 3D geometries such as rectangular and hexagonal reactor cores. The unstructured tetrahedron elements generated by Gambit are used to discretize the equations. Indeed, a key advantage of the unstructured tetrahedron elements is their superiority in mapping the curved boundaries or material interfaces in 3D geometries. In addition, the running time of computation code and the accuracy of the calculation may be optimized using proper unstructured tetrahedron elements. For several reasons, such as precision and simplicity, the Galerkin method has been used widely in the development of computer codes for solving diffusion or transport equations in different geometries [12,13]. The main advantage of the GFEM is that the definition of boundary conditions in this method is easier than that in the other methods [14]. The mentioned reasons convinced us to use the GFEM for solving the multigroup forward/adjoint neutron diffusion equation in 3D geometries.

An outline of the remainder of this contribution is as follows: In Section 2, we briefly introduce the numerical solution of the multigroup neutron diffusion equation in 3D geometries used to solve the forward/adjoint neutron diffusion equation. Section 3 presents the main specification of the IAEA-3D [15], VVER-1000 [16], and liquid metal fast breeder reactor (LMFBR) [17] benchmark problems. Numerical results and an analysis of the sensitivity of calculations to the

number of elements are presented in Section 4. In this section, we also discuss the results and advantages of applying the unstructured tetrahedron elements. Section 5 gives a summary and concludes the paper.

2. Numerical solution of the multigroup neutron diffusion equation in 3D geometries

2.1. *Forward neutron diffusion equation*

The multigroup neutron diffusion differential equation for steady state may be written as Eq. (1) [18,19]:

$$-D_g\nabla^2\phi_g(\bar{r})+\Sigma_{r,g}\phi_g(\bar{r})=\frac{\chi_g}{k_{eff}}\sum_{g=1}^{G}\nu\Sigma_{f,g'}\phi_{g'}(\bar{r})+\sum_{g\neq g}\Sigma_{s,g'\to g}\phi_{g'}(\bar{r})$$
$$g=1,2,\ldots,G \tag{1}$$

where all quantities were defined in the Nomenclature section of the present paper. The removal cross section ($\Sigma_{r,g}$) is the summation of the absorption and out-scattering cross sections. The removal cross section in the energy group g is expressed as $\Sigma_{r,g}=\Sigma_{a,g}+\sum_{g\neq g}\Sigma_{s,\,g\to g'}$.

Linear partial differential equations such as Eq. (1) may be solved using different numerical methods such as finite element, finite difference, and nodal. Here, the GFEM is used to discretize the neutron diffusion equation. To start the discretization, the whole solution volume is divided into the unstructured tetrahedron elements, as shown in Fig. 1. The advantage of the unstructured tetrahedron elements is their superiority in mapping any 3D geometry. The elements are generated using a Gambit mesh generator in FDNEUT format. After generating the desired geometry, the material type and boundary conditions are specified using the "Specify Continuum Types" and "Specify Boundary Types", respectively. Then, the geometry is divided into tetrahedron meshes using the "Mesh volume" section. To apply a size function while meshing a model, GAMBIT first divides the bounding box into a set of tetrahedron subsections and computes the size-function values at the corners of each subsection. To determine the size of any mesh element that exists within a given subsection, GAMBIT interpolates between the values assigned to the subsection corners. The total number of background-grid subsections affects the speed and accuracy of any size-function application. If the background grid contains only a few subsections, computational time is minimized, however, the computed mesh-element sizes might only crudely approximate the intended effects of the size function. Conversely, if the number of subsections is very large, the interpolated mesh-element sizes might accurately reflect the intended effects of the size function, but computational time might be prohibitive. The level to which GAMBIT divides the background grid by means of the TOOLS.SFUNCTION.BGRID_NONLINEAR_ERR_PERCENT default variable may be controlled. This default variable specifies the maximum allowable percentage difference between the exact and interpolated size-function values computed at the center of any subsection. If the difference exceeds the specified value for any subsection, GAMBIT further divides the subsection into a set of smaller subsections. Applying this method iteratively, GAMBIT subdivides the background grid until the percentage difference for all subsections is less than the specified maximum value.

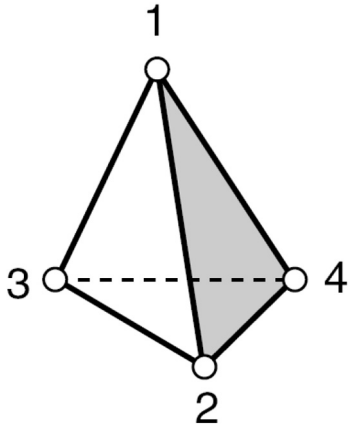

Fig. 1 – Unstructured tetrahedron elements.

In the linear approximation of shape function, the neutron flux in each element may be considered as Eq. (2) [14]:

$$\phi^{(e)}(x,y,z)=L_1(x,y,z)\phi_1+L_2(x,y,z)\phi_2+L_3(x,y,z)\phi_3+L_4(x,y,z)\phi_4 \tag{2}$$

where $L_i, i=1,2,3,4$ are the components of the shape function in Eq. (3):

$$\underline{N}^{(e)}(x,y,z)=[\,L_1(x,y,z)\quad L_2(x,y,z)\quad L_3(x,y,z)\quad L_4(x,y,z)\,] \tag{3}$$

The shape function components are defined as Eq. (4):

$$L_i(x,y,z)=\frac{a_i+b_ix+c_iy+d_iz}{6V};\quad i=1,2,3,4 \tag{4}$$

with

$$6V=\det\begin{bmatrix}1&x_1&y_1&z_1\\1&x_2&y_2&z_2\\1&x_3&y_3&z_3\\1&x_4&y_4&z_4\end{bmatrix} \tag{5}$$

in which, incidentally, the value V represents the volume of the tetrahedron. Expanding the other relevant determinants into their cofactors, we have

$$a_1=\det\begin{bmatrix}x_2&y_2&z_2\\x_3&y_3&z_3\\x_4&y_4&z_4\end{bmatrix}\quad b_1=-\det\begin{bmatrix}1&y_2&z_2\\1&y_3&z_3\\1&y_4&z_4\end{bmatrix}$$
$$c_1=-\det\begin{bmatrix}x_2&1&z_2\\x_3&1&z_3\\x_4&1&z_4\end{bmatrix}\quad d_1=-\det\begin{bmatrix}x_1&y_2&1\\x_2&y_3&1\\x_3&y_4&1\end{bmatrix} \tag{6}$$

with the other constants being defined by cyclic interchange of the subscripts in the order 1, 2, 3, 4.

The components of the shape function satisfy the criterion given in Eq. (7) at all points of the domain:

$$L_1(x,y,z)+L_2(x,y,z)+L_3(x,y,z)+L_4(x,y,z)=1 \tag{7}$$

The GFEM is a weighted residual method in which the purpose is to minimize the residual integral. In the weighted residual methods, the weighting function is considered as $W(r)=W^T\underline{N}(r)$. There are (at least) four submethods (collocation, subdomain, least squares, and Galerkin) for different

functions of W^T. Since W^T is a unit in the Galerkin method, the global shape function $[\underline{N}(r)]$ is considered a weighting function.

Multiplying Eq. (1) by the weighting function and integrating the results over the solution space, Eq. (8) is obtained:

$$\int_V dv W(r)\left(-D_g\nabla^2\phi_g(r) + \Sigma_{r,g}\phi_g(r) - \frac{\chi_g}{k_{eff}}\sum_{g'=1}^{G}\nu\Sigma_{f,g'}\phi_{g'}(r) - \sum_{g'\neq g}\Sigma_{s,g'\to g}\phi_{g'}(r)\right) = 0 \tag{8}$$

In the above equation, the differential part may be transformed, applying the divergence theorem, to Eq. (9):

$$\begin{aligned}\int_V dv W(r)\left(-D_g\nabla^2\phi_g(r)\right) &= \int_V dv\nabla W(r).\nabla\phi_g(r) - \int_V dv\nabla.\left(W(r)\nabla\phi_g(r)\right)\\ &= \int_V dv\nabla W(r).\nabla\phi_g(r) - \int_A ds W(r)\nabla\phi_g(r).\bar{n}\end{aligned} \tag{9}$$

where $\bar{n}$ is the normal unit vector on surface A. Two types of boundary conditions are considered in the calculation. The first boundary condition is no incoming neutrons at vacuum boundaries, which is expressed as Eq. (10):

$$\nabla\phi_g(r)\cdot\bar{n} = \frac{\partial\phi_g(r)}{\partial n} = -\frac{\phi_g(r)}{2D_g} \tag{10}$$

The second boundary condition is zero net current or perfectly reflective boundary condition, which is described by Eq. (11):

$$\frac{\partial\phi_g(r)}{\partial n} = 0 \tag{11}$$

Substituting the weighting function, Eqs. (9–11), and converting the integration on the reactor domain to the sum of the integrations on finite elements, the final form of Eq. (8) is obtained as Eq. (12):

$$\begin{aligned}&\sum_{e=1}^{E}\left[\int_V dv D_g\nabla\underline{N}^{(e)}(r)\nabla\underline{N}^{T(e)}(r)\phi_g^{(e)} + \Sigma_{r,g}^{(e)}\int_V dv\underline{N}^{(e)}(r)\underline{N}^{T(e)}(r)\phi_g^{(e)} + \int_A ds\underline{N}^{(e)}(r)\underline{N}^{T(e)}(r)\frac{\phi_g^{(e)}}{2}\right]\\ &= \sum_{e=1}^{E}\left[\frac{\chi_g}{k_{eff}}\sum_{g'=1}^{G}\nu\Sigma_{f,g'}\int_V dv\underline{N}^{(e)}(r)\underline{N}^{T(e)}(r)\phi_{g'}^{(e)} + \sum_{g'=1}^{g-1}\Sigma_{g'\to g}\int_V dv\underline{N}^{(e)}(r)\underline{N}^{T(e)}(r)\phi_{g'}^{(e)}\right]\end{aligned} \tag{12}$$

When element matrices have to be evaluated, it will follow that we are faced with the integration of quantities defined in terms of volume coordinates over the tetrahedron region. In this context, it is useful to note the following exact integration expression:

$$\int_V L_1^a L_2^b L_3^c L_4^d dx\,dy\,dz = \frac{a!b!c!d!}{(a+b+c+d+3)!}6V \tag{13}$$

We have encountered three types of integrals in solving Eq. (12). The first integral has appeared, as a result of applying the divergence theorem, as Eq. (14) [the first integral in the left-hand side of Eq. (12)]:

$$\int_V dv\nabla\underline{N}^{(e)}(r)\nabla\underline{N}^{T(e)} = \frac{1}{36V^{(e)}}\begin{bmatrix} b_1^{(e)}b_1^{(e)}+c_1^{(e)}c_1^{(e)}+d_1^{(e)}d_1^{(e)} & b_1^{(e)}b_2^{(e)}+c_1^{(e)}c_2^{(e)}+d_1^{(e)}d_2^{(e)} & b_1^{(e)}b_3^{(e)}+c_1^{(e)}c_3^{(e)}+d_1^{(e)}d_3^{(e)} & b_1^{(e)}b_4^{(e)}+c_1^{(e)}c_4^{(e)}+d_1^{(e)}d_4^{(e)}\\ b_2^{(e)}b_1^{(e)}+c_2^{(e)}c_1^{(e)}+d_2^{(e)}d_1^{(e)} & b_2^{(e)}b_2^{(e)}+c_2^{(e)}c_2^{(e)}+d_2^{(e)}d_2^{(e)} & b_2^{(e)}b_3^{(e)}+c_2^{(e)}c_3^{(e)}+d_2^{(e)}d_3^{(e)} & b_2^{(e)}b_4^{(e)}+c_2^{(e)}c_4^{(e)}+d_2^{(e)}d_4^{(e)}\\ b_3^{(e)}b_1^{(e)}+c_3^{(e)}c_1^{(e)}+d_3^{(e)}d_1^{(e)} & b_3^{(e)}b_2^{(e)}+c_3^{(e)}c_2^{(e)}+d_3^{(e)}d_2^{(e)} & b_3^{(e)}b_3^{(e)}+c_3^{(e)}c_3^{(e)}+d_3^{(e)}d_3^{(e)} & b_3^{(e)}b_4^{(e)}+c_3^{(e)}c_4^{(e)}+d_3^{(e)}d_4^{(e)}\\ b_4^{(e)}b_1^{(e)}+c_4^{(e)}c_1^{(e)}+d_4^{(e)}d_1^{(e)} & b_4^{(e)}b_2^{(e)}+c_4^{(e)}c_2^{(e)}+d_4^{(e)}d_2^{(e)} & b_4^{(e)}b_3^{(e)}+c_4^{(e)}c_3^{(e)}+d_4^{(e)}d_3^{(e)} & b_4^{(e)}b_4^{(e)}+c_4^{(e)}c_4^{(e)}+d_4^{(e)}d_4^{(e)}\end{bmatrix} \tag{14}$$

where parameters a_i, b_i, c_i, and d_i have been defined in Eq. (6)

The solution of the second integral on the left-hand side of Eq. (12) and all integrals on the right-hand side of Eq. (12) are given in Eq. (15):

$$\int_V dv\underline{N}^{(e)}(r)\underline{N}^{T(e)} = 6V^{(e)}\begin{bmatrix}\frac{1}{60}&\frac{1}{120}&\frac{1}{120}&\frac{1}{120}\\ \frac{1}{120}&\frac{1}{60}&\frac{1}{120}&\frac{1}{120}\\ \frac{1}{120}&\frac{1}{120}&\frac{1}{60}&\frac{1}{120}\\ \frac{1}{120}&\frac{1}{120}&\frac{1}{120}&\frac{1}{60}\end{bmatrix} \tag{15}$$

The solution of the last form of integrals appeared in Eq. (12) [the third integral in the left-hand side of Eq. (12)] is given as Eq. (16):

$$\int_A ds\underline{N}^{(e)}(r)\underline{N}^{T(e)} = 2\Delta^{(e)}\begin{bmatrix}\frac{1}{12}&\frac{1}{24}&\frac{1}{24}&0\\ \frac{1}{24}&\frac{1}{12}&\frac{1}{24}&0\\ \frac{1}{24}&\frac{1}{24}&\frac{1}{12}&0\\ 0&0&0&0\end{bmatrix} \tag{16}$$

Eq. (16) is the local boundary condition matrix for each element in the situation when there is no incoming current. Eq. (16) is a zero matrix for net current boundary conditions.

Assembling the local matrices, Eqs. (14–16), into the global matrix, the system of equations, which is an eigenvalue problem, is obtained. Here, the eigenvalue problem is solved using the power iteration method. In the first step, a guess is considered for neutron multiplication factor ($k_{eff}^{(0)}$) and neutron flux distributions ($\phi_g^{(0)}$) in each energy group. The unit vector and the value of $k_{eff}^{(0)} = 1$ are considered as an initial guess. The initial fission source is calculated as $S_f^{(0)}(r) = \sum_{g=1}^{G}\nu\Sigma_{f,g}(r)\,\phi_g^{(0)}(r)$. In the second step, the neutron diffusion equation is solved using the GFEM by considering

the flat approximation for neutron flux distribution. The calculated neutron flux vector and neutron multiplication factor are used in the next iteration of the calculation: update the fission integral as $S_f^{(n)}(r) = \sum_{g=1}^{G} \nu\Sigma_{f,g}(\bar{r})\,\phi_g^{(n)}(r)$. The eigenvalue of the problem is defined as $k_{eff}^{(n)} = k_{eff}^{(n-1)} \int_{\Omega} d\Omega\, S_f^{(n)}(r) / \int_{\Omega} d\Omega\, S_f^{(n-1)}(r)$, where n denotes the iteration number. In the next step, the values of $k_{eff}^{(n)}$ and $\phi_g^{(n)}$ were compared with those of $k_{eff}^{(n-1)}$ and $\phi_g^{(n-1)}$ for all energy groups. If the changes are greater than a prescribed tolerance, then calculations are performed in the next iteration; otherwise, the iteration is completed.

The output of the present section is the calculation of the neutron multiplication factor and neutron flux distribution in each energy group. Power distribution in the reactor core may be calculated if the neutron flux distribution is determined.

2.2. Adjoint diffusion equation

To solve the adjoint diffusion equation, it is noted that the adjoint operator is the transpose of the direct operator [18,20]. To this end, Eq. (1) is formed in a matrix notation as Eq. (17):

$$L\phi = \frac{1}{k_{eff}} F\phi \tag{17}$$

where L is a loss operator and F a fission operator.

Therefore, the matrix form of the adjoint diffusion equation is written as Eq. (18):

$$L^{\dagger}\phi^{\dagger} = \frac{1}{k_{eff}^{\dagger}} F^{\dagger}\phi^{\dagger} \tag{18}$$

Here, $L^{\dagger}$ and $F^{\dagger}$ are the transpose of the L and F, respectively [19]. In addition, $\phi^{\dagger}$ and $k_{eff}^{\dagger}$ refer to adjoint flux and adjoint multiplication factor, respectively. To solve the adjoint diffusion equation, the same method that was applied to the forward diffusion equation is used. The algorithm presented in the previous subsection for solving the system of equations is also applied. The adjoint multiplication factor and adjoint flux in each energy group are obtained from the calculation.

2.3. Neutron fixed source equation

The forward/adjoint neutron diffusion equations investigated in the previous two subsections are the criticality problems. In the present section, the solution to the neutron fixed source problem is obtained. The general matrix form of the neutron fixed source equation is given as Eq. (19):

$$L\phi = S \tag{19}$$

where L and S are loss operator and external neutron source, respectively.

In addition to the integrals mentioned in Eqs. (16)–(18), we encounter a new form of integral in the discretization of Eq. (19) using the GFEM. The solution to local integrals that appeared due to the presence of a volumetric external source is given as Eq. (20):

$$\int_V d\nu \underline{N}^{(e)}(r) = 6V^{(e)} \begin{bmatrix} \frac{1}{24} \\ \frac{1}{24} \\ \frac{1}{24} \\ \frac{1}{24} \end{bmatrix} \tag{20}$$

The system of equations may be obtained from assembling the calculated local matrices for each element. The solution of the system of equations gives the neutron flux distribution for each energy group in the different regions.

3. Main specification of the benchmark problems

3.1. Criticality benchmark problems

3.1.1. IAEA-3D PWR

The IAEA-3D PWR problem has been a very important standard benchmark problem to measure the performance of calculation methods for neutronics [15]. A total of 177 fuel assemblies, including nine fully rodded fuel assemblies and four rodded fuel assemblies, compose the core; 64 reflector assemblies surround the core. The fuel assembly pitch is 20 cm and the active height of a fuel assembly is 340 cm. The thickness of the axial reflector is 20 cm. Fig. 2 displays one-eighth of the IAEA-3DPWR. The boundary conditions of the reactor core are no incoming current for the external boundaries and perfectly reflective boundary condition for the symmetry lines. Table 1 represents the material cross section of each assembly for the IAEA-3D reactor core.

3.1.2. VVER-1000

VVER-1000 is the second benchmark problem in this study [16]. The radial fuel assembly lattice pitch is 24.1 cm. This corresponds to the prototype VVER-1000 and is slightly different from the actual Fuel Assembly (FA) pitch of 23.6 cm in VVER-1000/V320; however, it is acceptable for a mathematical benchmark. The core height is 355 cm, covered with axial and radial reflectors. The total height is 426 cm, including 35.5 cm thick axial reflectors. Fig. 3 shows 1/12 of the benchmark core configuration. The boundary conditions of the reactor core include no incoming current for the external boundaries and perfectly reflective boundary condition for the symmetry lines. The material cross section of each assembly for VVER-1000 is given in Table 2.

3.1.3. LMFBR configuration in R–Z geometry

To validate the results obtained from the solution of the neutron diffusion equation against the P_1 approximation of the neutron transport theory, we consider the multigroup LMFBR benchmark problem in R–Z geometry [17]. The material cross section for this problem is given in Table 3. The neutron diffusion coefficient may be obtained from the total cross section as $D = \frac{1}{3\sum_t}$. The reactor is a right circular cylinder. This is obtained by rotating the system shown in Fig. 4

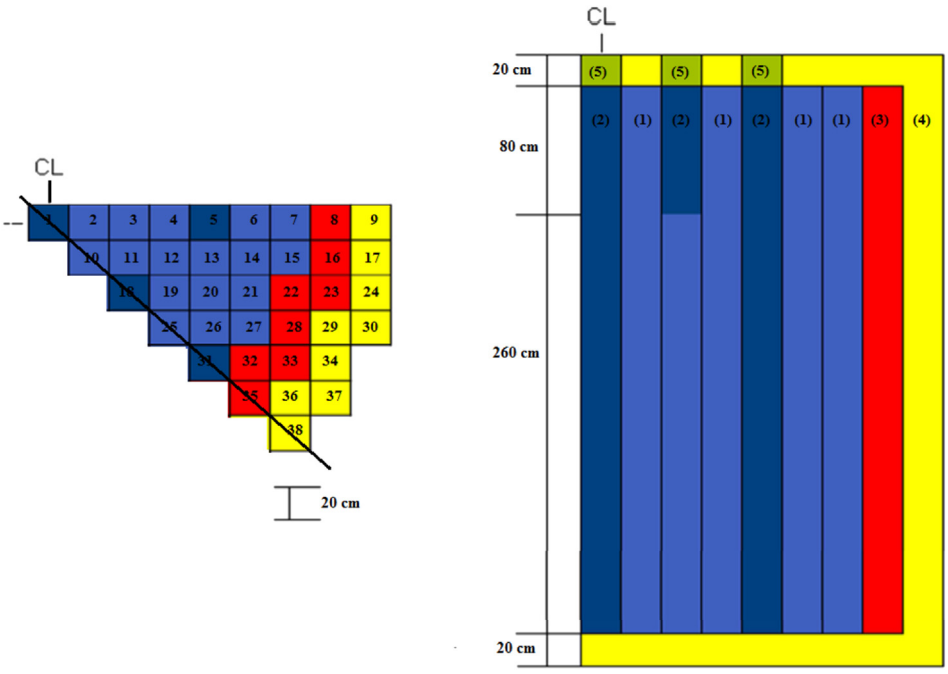

Fig. 2 – One-eighth of the IAEA-3D Pressurized Water Reactor (PWR) core [15]. CL, Central Line.

Table 1 – Material cross section of each assembly for the IAEA-3D reactor core.

(5)	(4)	(3)	(2)	(1)	Cross section
2.000	2.000	1.500	1.500	1.500	$\Sigma_{s,1\to2}$
0.300	0.300	0.400	0.400	0.400	D_1(cm)
0.000	0.000	0.000	0.000	0.000	$\nu\Sigma_{f,1}(/\mathrm{cm})$
0.000	0.000	0.135	0.135	0.135	$\nu\Sigma_{f,2}(/\mathrm{cm})$
0.000	0.000	0.010	0.010	0.010	$\Sigma_{a,1}(/\mathrm{cm})$
0.055	0.010	0.130	0.085	0.080	$\Sigma_{a,2}(/\mathrm{cm})$
0.040	0.040	0.020	0.020	0.020	$\Sigma_{s,1\to2}(/\mathrm{cm})$

3D, three dimensional.

about the Y-axis. Thus, we obtain a cylindrical reactor of height 338.4 cm and radius 123.45 cm.

3.2. *Neutron fixed source benchmark problems*

The neutron fixed source equation may be solved in any 3D and hexagonal geometries. Since the author could not find any validated neutron fixed source benchmark problems, a simple problem was considered to validate the calculation. Here, we have presented a problem to validate the neutron fixed source problem. Fig. 5 shows the multiregion cube with the known material and unit volumetric neutron sources located in Regions 1 and 9. The dimension of the considered cube is 30 cm × 30 cm × 10 cm. The material cross section of each assembly for the considered cube is given in Table 4. The

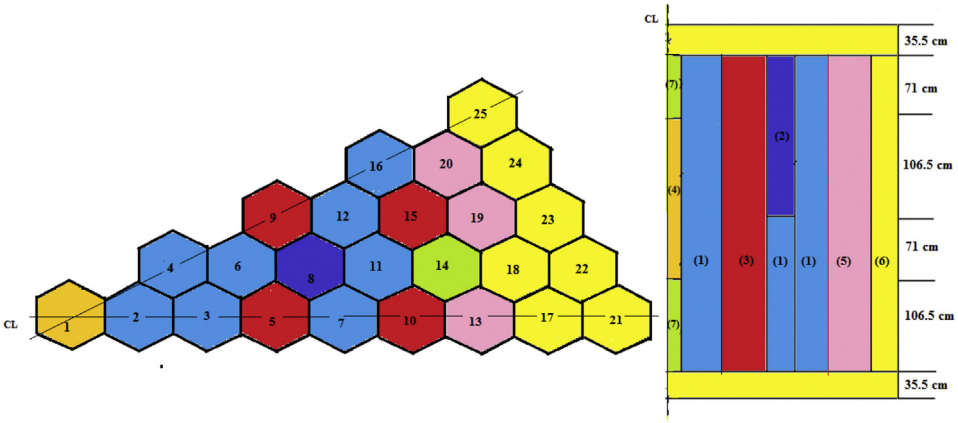

Fig. 3 – One-twelfth of the VVER-1000 reactor core [16]. CL, Central Line.

Table 2 – Material cross section of each assembly for the VVER-1000 reactor core.

(7)	(6)	(5)	(4)	(3)	(2)	(1)	Cross section
1.369	1.000	1.369	1.394	1.371	1.409	1.375	$\Sigma_{s,1\to2}$
0.379	0.333	0.379	0.385	0.380	0.388	0.383	D_1(cm)
0.006	0.000	0.006	0.006	0.006	0.005	0.005	$\nu\Sigma_{f,1}(/\mathrm{cm})$
0.126	0.000	0.130	0.126	0.115	0.084	0.084	$\nu\Sigma_{f,2}(/\mathrm{cm})$
0.009	0.016	0.009	0.010	0.009	0.010	0.008	$\Sigma_{a,1}(/\mathrm{cm})$
0.086	0.053	0.088	0.095	0.080	0.075	0.066	$\Sigma_{a,2}(/\mathrm{cm})$
0.015	0.025	0.015	0.014	0.015	0.014	0.016	$\Sigma_{s,1\to2}(/\mathrm{cm})$

Table 3 – Material cross section of each assembly in the LMFBR.

$\Sigma_{s,1\to2}(/\mathrm{cm})$	$\Sigma_{a,2}(/\mathrm{cm})$	$\Sigma_{a,1}(/\mathrm{cm})$	D_2(cm)	D_1(cm)	Regions
0.400	0.131	0.026	0.483	1.365	1–9

LMFBR, liquid metal fast breeder reactor.

boundary condition for the entire surface is no incoming neutron current.

4. Numerical results and discussion

First, we present the results for the IAEA-3D reactor. Fig. 6 shows the IAEA-3D with unstructured tetrahedron elements. Table 5 shows the calculated forward and adjoint multiplication factors versus the number of the unstructured tetrahedron elements. In Fig. 7, power distribution in the reactor core has been compared with the reference data [15]. The reference values was calculated using the finite difference method with the VENTURE computational code [21]. The data used as reference in the present study were obtained by extrapolation of results of the VENTURE computational code. Extrapolation of results is done on the basis of error dependence on the square of the mesh spacing [15].

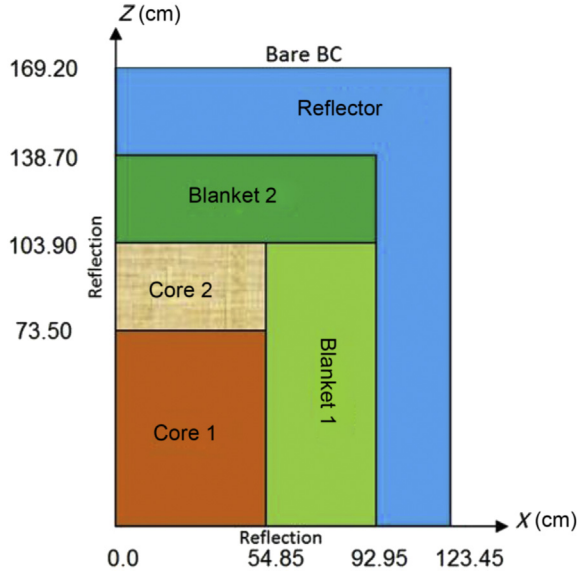

Fig. 4 – View of 1/8 of the LMFBR [17]. BC, boundary condition; LMFBR, liquid metal fast breeder reactor.

The same results for the VVER-1000 reactor have been repeated in Table 6 and Fig. 8. In Fig. 8, the calculated power distribution in the reactor core has been compared with the reference data [16]. The reference values for the Schulz benchmark were calculated using the CRONOS computational code [22] and with the extrapolated finite element solution of second order with Lagrange polynomials on triangular-z meshes. CRONOS is a reactor code of Commissariat à l'EnergieAtomique (CEA), which uses finite elements and nodal methods for homogenized diffusion and transport calculations; the code also has 3D kinetics and pin-by-pin diffusion modules. The approximation in the hexagonal plane uses the Gauss–Legendre numerical quadrature corresponding to superconvergent finite elements. The discretization was performed by considering 54 triangles per hexagon and Nz = 24 meshes in the axial direction [16].

As shown in Tables 5 and 6, the calculations have been performed for different numbers of elements in order to analyze the sensitivity of the calculations to number the elements. As expected, the difference between the calculated forward/adjoint multiplication factor and the reference value decreases as the number of elements is increased. The minimum RPE [defined as Eq. (21)] is 0.0136 for 540,130 elements in

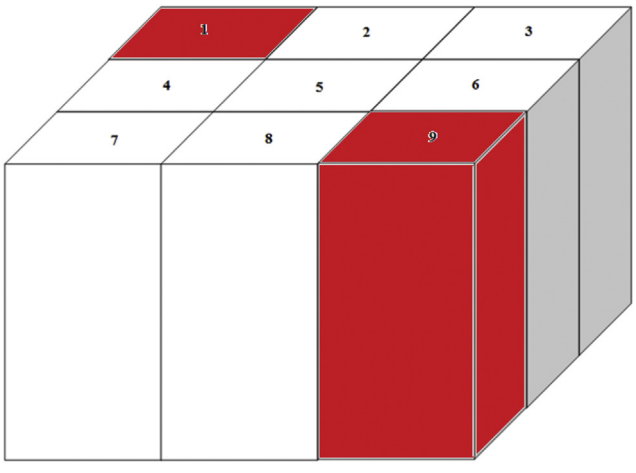

Fig. 5 – The cube considered for validation of neutron fixed source problem.

Table 4 – Material cross section of each assembly for the considered cube.

Region	Cross section (/cm)	Energy group			
		1	2	3	4
Core 1	$\sum_t$	0.116757	0.221928	0.348579	0.350966
	$\nu\sum_f$	0.017811	0.004777	0.00632	0.024478
	$\sum_{s,g\to g'}$				
	g	0.07235	0.03767	0.00019	0
		0	0.21435	0.00416	3E−07
		0	0	0.33785	0.001801
		0	0	0	0.32258
Core 2	$\sum_t$	0.116695	0.221781	0.348871	0.35633
	$\nu\sum_f$	0.019505	0.006108	0.008089	0.031306
	$\sum_{s,g\to g'}$				
	g	0.07238	0.03709	0.00018	1.36E−08
		0	0.21375	0.00415	3.08E−08
		0	0	0.33741	0.001803
		0	0	0	0.324236
Blanket 1	$\sum_t$	0.12268	0.234088	0.363161	0.345218
	$\nu\sum_f$	0.014126	0.000838	0.001073	0.004205
	$\sum_{s,g\to g'}$				
	g	0.07493	0.04196	0.00022	0
		0	0.22763	0.00431	1.76E−07
		0	0	0.35443	0.001793
		0	0	0	0.329045
Blanket 2	$\sum_t$	0.132588	0.256029	0.38695	0.369594
	$\nu\sum_f$	0.017301	0.001358	0.001767	0.00692
	$\sum_{s,g\to g'}$				
	g	0.07909	0.04652	0.00025	0
		0	0.24868	0.00469	6.09E−07
		0	0	0.37668	0.001905
		0	0	0	0.34972
Outer reflector	$\sum_t$	0.11317	0.177615	0.36705	0.411535
	$\sum_{s,g\to g'}$				
	g	0.08232	0.03028	0.00007	0
		0	0.17456	0.00282	0
		0	0	0.36419	0.00163
		0	0	0	0.407033
Fission spectrum		0.588153	0.40819	0.003638	1.95E−05

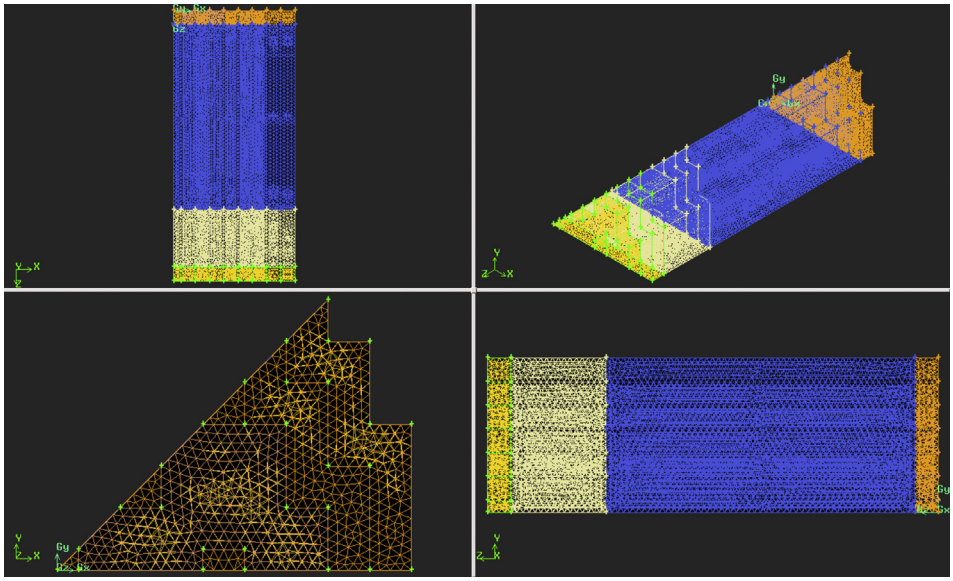

Fig. 6 – View of IAEA-3D with unstructured tetrahedron elements.

Table 5 – Calculated forward/adjoint multiplication factor for IAEA-3D reactor core.

Number of elements	Unknowns	k_{eff}	$k^{\dagger}_{eff}$	RPE(%)
36,629	6,597	1.03093	1.03093	0.1846
41,691	8,690	1.03061	1.03061	0.1535
43,262	9,008	1.03047	1.03047	0.1399
51,017	10,471	1.02998	1.02998	0.0923
67,204	13,581	1.02965	1.02965	0.0603
81,826	16,430	1.02963	1.02963	0.0583
154,407	29,541	1.02936	1.02936	0.0321
276,650	47,932	1.02926	1.02926	0.0224
341,457	59,092	1.02922	1.02922	0.0185
540,130	92,821	1.02917	1.02917	0.0136

The reference effective multiplication factor is $k_{eff} = 1.02903$ [15].
3D, three dimensional; RPE, Relative Percent Error.

Table 6 – Calculated forward/adjoint multiplication factor for VVER-1000.

Number of elements	Unknowns	k_{eff}	$k^{\dagger}_{eff}$	RPE(%)
30,148	4,932	1.05156	1.05156	0.1934
35,412	6,345	1.05101	1.05101	0.1410
47,612	7,805	1.05078	1.05078	0.1191
51,467	9,165	1.05034	1.05034	0.0772
58,120	11,910	1.05003	1.05003	0.0476
66,796	13,256	1.04994	1.04994	0.0391
76,096	16,256	1.04982	1.04982	0.0276
101,245	20,789	1.04976	1.04976	0.0219
163,216	31,248	1.04970	1.04970	0.0162
297,643	45,789	1.04961	1.04961	0.0076

The reference effective multiplication factor is $k_{eff} = 1.04953$ [16].
RPE, Relative Percent Error.

IAEA-3D. The same parameter is 0.0076 for 297,643 elements in VVER-1000. The calculated RPEs for the forward multiplication factor and power distribution in the present study are in the range of other same reported results [15,23].

$$\mathrm{RPE}(\%) = \frac{\text{calculated value} - \text{reference value}}{\text{reference value}} \times 100 \qquad (21)$$

As expected, the calculated forward and adjoint multiplication factors are the same when the considered accuracy is five decimal digits.

To compare the results obtained from the solution of the neutron diffusion equation with the neutron transport equation, the LMFBR is considered. The neutron multiplication factor obtained from the solution of the neutron diffusion equation using GFEM-3D is compared with the reference data, in which the neutron transport equation was solved using quadratic finite element P_1 approximation [17]. Fig. 9 shows the LMFBR with unstructured tetrahedron elements. Table 7 shows the comparison between the calculated neutron multiplication factors for different numbers of elements and the reference values. As expected, the difference between the calculated neutron multiplication factor and the reference value decreases as the number of elements is increased. In addition, Table 8 displays the comparison between the

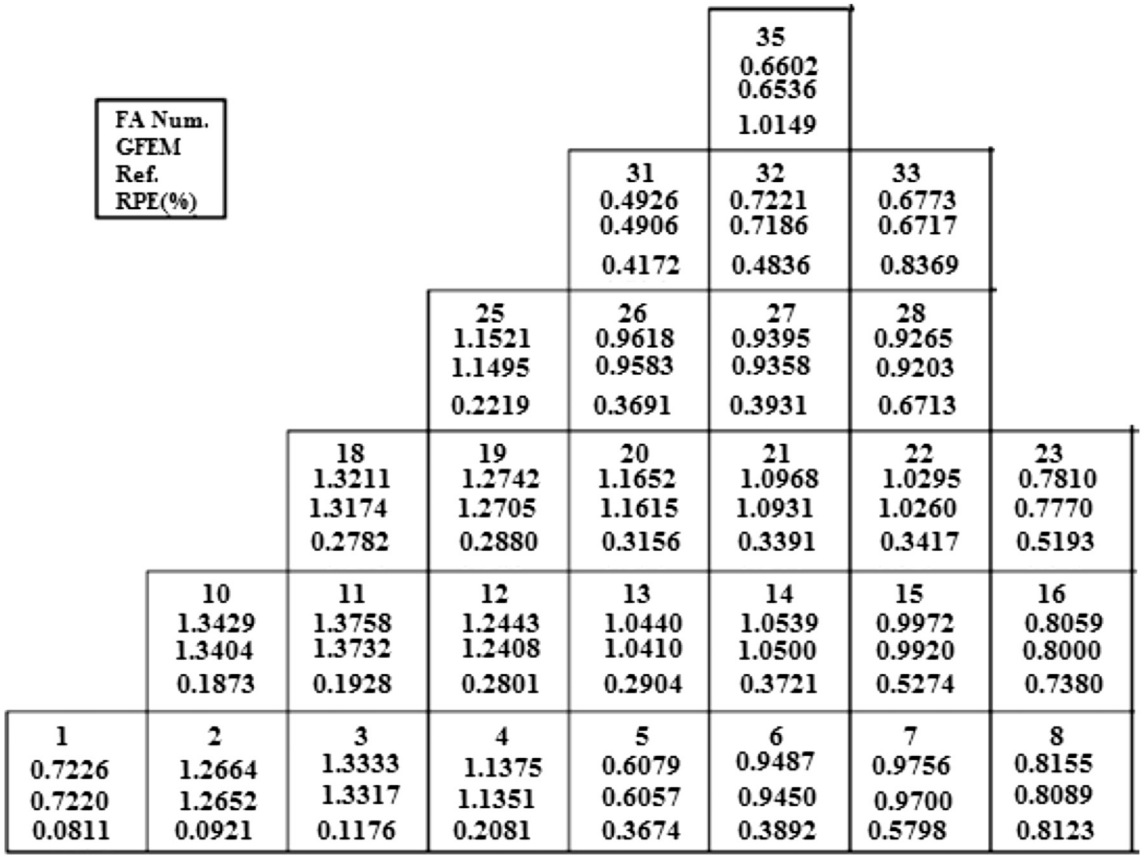

Fig. 7 – Power distribution in the IAEA-3D reactor core. GFEM, Galerkin finite element method.; FA Num., Fuel Assembly Number; RPE, Relative Percent Error; Ref., Reference.

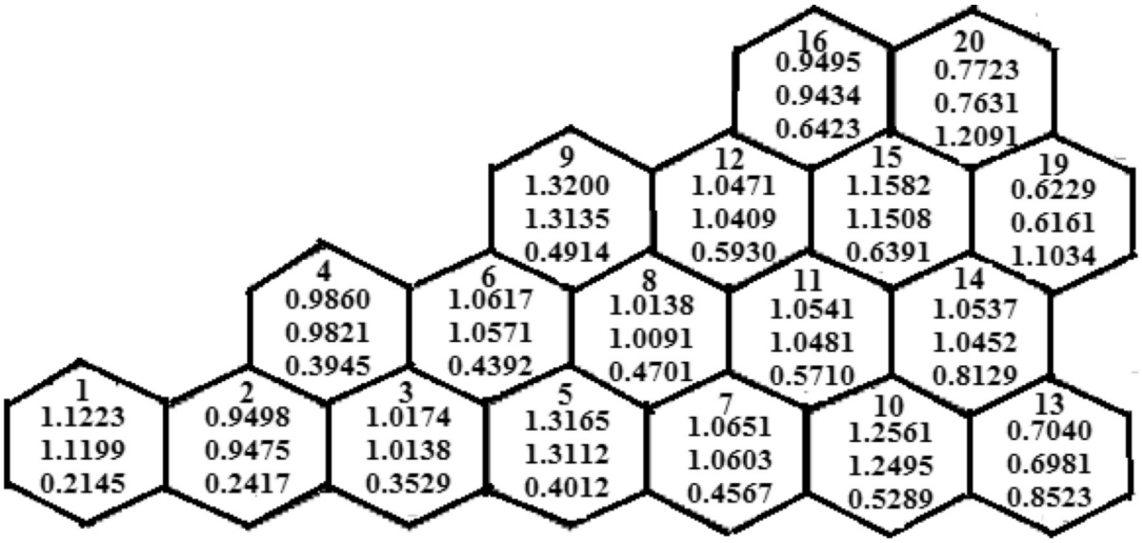

Fig. 8 – Power distribution in the VVER-1000 reactor core.

averaged neutron flux in each region and the reference value. The reference data are obtained through the solution of the multigroup neutron transport equation with quadratic elements and P_1 approximation. Since the solution of P_1 approximation of the neutron transport equation using high-order finite elements is compared with the results of linear approximation of the GFEM for solution of the neutron diffusion equation, the obtained errors are within acceptable ranges.

In the aforementioned calculation, the unstructured tetrahedron elements generated by Gambit software have been used. The advantage of these elements is their superiority in mapping any 3D geometry. In addition, as discussed by the author in a previously published work [12], an acceptable level of accuracy with a low computational cost may be achieved using the unstructured elements.

To validate the performed calculation for the neutron fixed source problem, the results of GFEM-3D and CITATION [24] computational codes have been compared. Since the calculation has been performed using small meshes in the CITATION computational code, the obtained neutron flux distribution from CITATION may be considered as reference data. The calculated neutron flux distributions in a layer with $z = 5$ cm are compared in Table 9. As shown, the neutron flux calculated using GFEM-3D has a good agreement with the results of the CITATION computation code.

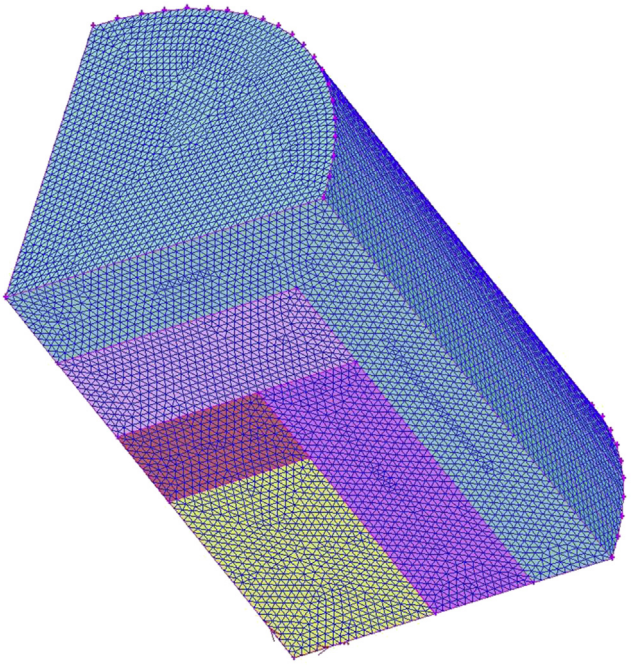

Fig. 9 – View of the LMFBR with unstructured tetrahedron elements. LMFBR, liquid metal fast breeder reactor.

5. Conclusion

In the present study, the GFEM-3D computational code was developed to solve the multigroup neutron diffusion equation based on the GFEM. Both the criticality and neutron fixed source calculations may be performed using the computational code developed. The calculations were performed using the unstructured tetrahedron elements for hexagonal, rectangular, and cylindrical 3D geometries. The forward/adjoint multiplication factor, and forward/adjoint flux and power

Table 7 – Calculated neutron multiplication factor for the LMFBR.

Number of elements	Unknowns	k_{eff}	Absolute error
68,109	11,993	0.93860	−0.00172
95,669	16,767	0.93890	−0.00142
204,763	35,450	0.93919	−0.00113
394,076	67,869	0.93930	−0.00102
1,594,051	270,628	0.93954	−0.00078

The reference effective multiplication factor is $k_{eff} = 0.94032$ [17].
LMFBR, liquid metal fast breeder reactor.

Table 8 – Calculated group-average neutron fluxes for the LMFBR.

Region	ϕ_1		ϕ_2		ϕ_2		ϕ_3	
	P_1[a]	GFEM-3D	P_1	GFEM-3D	P_1	GFEM-3D	P_1	GFEM-3D
Core 1	1.176×10^{-5}	1.181×10^{-5}	9.227×10^{-5}	9.243×10^{-5}	3.400×10^{-5}	3.429×10^{-5}	2.165×10^{-6}	2.319×10^{-6}
Core 2	9.624×10^{-6}	9.702×10^{-6}	6.851×10^{-5}	6.864×10^{-5}	2.382×10^{-5}	2.394×10^{-5}	1.414×10^{-6}	1.497×10^{-6}
Blanket 1	1.129×10^{-6}	1.089×10^{-6}	1.767×10^{-5}	1.776×10^{-5}	9.355×10^{-6}	9.495×10^{-6}	1.021×10^{-6}	1.118×10^{-6}
Blanket 2	7.178×10^{-7}	6.916×10^{-7}	1.037×10^{-5}	1.058×10^{-5}	5.195×10^{-6}	5.268×10^{-6}	5.240×10^{-7}	6.843×10^{-7}
Reflector	3.426×10^{-8}	2.532×10^{-8}	1.595×10^{-6}	1.761×10^{-6}	1.353×10^{-6}	1.501×10^{-6}	3.044×10^{-7}	4.126×10^{-7}

GFEM, Galerkin finite element method; LMFBR, liquid metal fast breeder reactor; 3D, three dimensional.
[a] The results obtained from the solution of the P_1 approximation using quadratic finite elements [17].

Table 9 – Comparison between the calculated neutron flux distribution using the CITATION and GFEM-3D computational codes.

Neutron flux in Energy Group 2		Neutron flux in Energy Group 1		Region
CITATION	GFEM-3D	CITATION	GFEM-3D	
0.3239	0.3199	4.2156	4.1831	1
0.0866	0.0866	0.8319	0.8357	2
0.0040	0.0040	0.0330	0.0327	3
0.0866	0.0866	0.8319	0.8359	4
0.0326	0.0326	0.2672	0.2676	5
0.0026	0.0026	0.0205	0.0203	6
0.0040	0.0040	0.0329	0.0327	7
0.0026	0.0026	0.0205	0.0203	8
0.0004	0.0004	0.0035	0.0035	9

GFEM, Galerkin finite element method; 3D, three dimensional.

distributions are the outputs of the calculation performed by the GFEM-3D computation code.

To validate the calculations, an analysis of 3D benchmark reactor cores was carried out and the obtained results were compared with the reference data. In both IAEA-3D and VVER-1000 reactors, acceptable results for the neutron multiplication factor and power distribution were obtained. To validate the present calculation against the multigroup neutron transport theory, the obtained results for the LMFBR were compared with the results of P_1 approximation [17]. The neutron fixed source problem was also validated through a comparison of the neutron flux distributions calculated by the GFEM-3D and CITATION computational codes.

A reader can conclude that the developed computer code is a reliable tool for deterministic static calculations of both thermal and fast 3D reactor cores. It is applicable to full-core fuel management and design application studies of nuclear reactor cores.

Conflicts of interest

The author has no conflict of interest.

Acknowledgments

The author is grateful to the Advanced Nuclear Computational Center of Iran for financially supporting the present work. The author also thanks Mr Yousefi for cooperation in the preparation of data for the LMFBR benchmark problem.

Nomenclature

$\phi_g(r)$	Forward flux in energy group g
$\phi_g^{\dagger}(r)$	Adjoint flux in energy group g
k_{eff}	Forward neutron multiplication factor
$k_{\text{eff}}^{\dagger}$	Adjoint multiplication factor
χ_g	Neutron spectrum in energy group g
D_g	Diffusion constant in energy group g
$\Sigma_{r,g}$	Macroscopic removal cross section in energy group g
$\Sigma_{f,g}$	Macroscopic fission cross section in energy group g
$\Sigma_{s,g' \to g}$	Macroscopic scattering cross section from energy group g' to g
ν	Fission neutron yield
∇	Nabla operator

REFERENCES

[1] L.F. Richardson, The approximate arithmetical solution by finite differences of physical problems involving differential equations, with an application to the stresses in a masonry dam, Philos. Trans. R. Soc. Lon. A 210 (1911) 307–357.
[2] K. Ivanov, M. Manolova, T. Apostolov, An effective solution scheme of a three-dimensional reactor core model in hexagonal geometry, Comput. Phys. Commun. 82 (1994) 1–16.
[3] V.G. Zimin, D.M. Baturin, Polynomial nodal method for solving neutron diffusion equations in hexagonal-z geometry, Ann. Nucl. Energy 29 (2002) 1105–1117.
[4] A. Hébert, Development of the nodal collocation method for solving the neutron diffusion equation, Ann. Nucl. Energy 14 (1987) 527–541.
[5] K.S. Smith, An Analytic Nodal Method for Solving the Two-Group, Multidimensional, Static and Transient Neutron Diffusion Equations, Massachusetts Institute of Technology, Cambridge, United States, 1979.
[6] T.J. Barth, Aspects of unstructured grids and finite-volume solvers for the Euler and Navier–Stokes equations, AGARD, Special Course on Unstructured Grid Methods for Advection Dominated Flows 61, NASA Ames Research Center, Moffett Field, CA, United States, 1992, pp. 18–34. SEE N92-27671.
[7] R. Li, Z. Chen, W. Wu, Generalized Difference Methods for Differential Equations: Numerical Analysis of Finite Volume Methods, CRC Press, United States, 2000.
[8] S. Iqbal, An Adaptive Finite Element Formulation of the Boltzmann-Type Neutron Transport Equation, Ph.D thesis, Ghulam Ishaq Khan Institute of Engineering Sciences and Technology, Topi, Pakistan, 2007.
[9] A. Hébert, A Raviart–Thomas–Schneider solution of the diffusion equation in hexagonal geometry, Ann. Nucl. Energy 35 (2008) 363–376.

[10] S. Cavdar, H. Ozgener, A finite element/boundary element hybrid method for 2-D neutron diffusion calculations, Ann. Nucl. Energy 31 (2004) 1555–1582.
[11] Y. Wang, W. Bangerth, J. Ragusa, Three-dimensional *h*-adaptivity for the multigroup neutron diffusion equations, Prog. Nucl. Energy 51 (2009) 543–555.
[12] S.A. Hosseini, N. Vosoughi, Development of two-dimensional, multigroup neutron diffusion computer code based on GFEM with unstructured triangle elements, Ann. Nucl. Energy 51 (2013) 213–226.
[13] M. Maiani, B. Montagnini, A Galerkin approach to the boundary element-response matrix method for the multigroup neutron diffusion equations, Ann. Nucl. Energy 31 (2004) 1447–1475.
[14] J. Zhu, Z. Taylor, O. Zienkiewicz, The Finite Element Method: Its Basis and Fundamentals, Butterworth-Heinemann, Barcelona, Spain, 2005.
[15] A.C. Center, Benchmark Problem Book, Report ANL-7416 (Suppl. 2), Argonne National Laboratory, Argonne, IL, 1977.
[16] G. Schulz, Solutions of a 3D VVER-1000 Benchmark, in: Proceedings of the 6th Symposium of AER on VVER Reactor Physics and Safety, Kirkkonummi, Finland, 1996.
[17] J. Wood, C. De Oliveira, A multigroup finite-element solution of the neutron transport equation—I: *XY* geometry, Ann. Nucl. Energy 11 (1984) 229–243.
[18] J.J. Duderstadt, L.J. Hamilton, Nuclear Reactor Analysis, John Wiley & Sons, Inc, 1976.
[19] J.R. Lamarsh, Introduction to Nuclear Reactor Theory, Addison-Wesley, Reading, MA, 1966.
[20] G.L. Bell, S. Glasstone, Nuclear Reactor Theory, Van Nostrand Reinhold, New York, 1970.
[21] D. Vondy, VENTURE—A Code Block for Solving Multigroup Neutronic Problems Applying Finite Difference Diffusion Approximation to Neutron Transport, 1977. ORNL-5062R1.
[22] J. Lautard, S. Loubiere, C. Fedon-Magnaud, Cronos: A Modular Computational System for Neutronic Core Calculations, 1992.
[23] S. González-Pintor, D. Ginestar, G. Verdú, High order finite element method for the lambda modes problem on hexagonal geometry, Ann. Nucl. Energy 36 (2009) 1450–1462.
[24] T. Fowler, D. Vondy, G. Cunningham, Nuclear reactor core analysis code; CITATION, ORNL-TM-2496, Rev. 2, Oak Ridge National Laboratory, Oak Ridge, TN, July 1971.